International Journal of Electrical and Computer Engineering (IJECE)
Vol. 4, No. 1, Feburary 2014, pp. 52~63
ISSN: 2088-8708

A New Approach for Broken Bar Fault Detection in Three-Phase Induction Motor Using Instantaneous Power Monitoring under Low Slip Range

Yassine Maouche, Mohamed El Kamel Oumaamar, Mohamed Boucherma, and Abdelmalek Khezzar
Laboratoire d'´ electrotechnique de Constantine

Article Info

Article history:

Received Oct 2, 2013
Revised Nov 13, 2013
Accepted Dec 10, 2013

Keyword:

Broken bar fault
Condition monitoring
Fault detection
Fault diagnosis
Fourier transforms
Spectrum analysis

ABSTRACT

The majority of research is about the detection of broken bar fault in three-phase induction motor at high slip. Thus, it becomes very interesting and demanding to detect faults in case of low slip range. In this study, a novel investigation of broken bar faults using instantaneous power is presented. The method is based on calculations and frequency analysis of partial and total instantaneous power under low slip range. The used model of squirrel cage induction machine takes into account the geometry and winding layout. This model will be used to analyze the impact of broken bar on instantaneous power spectrum. The proposed ideas in this paper are verified experimentally. The results show that broken bar fault can be more reliably detected under low slip range when using a large frequency area of both partial and total instantaneous power spectrums.

Corresponding Author:

Yassine Maouche
Laboratoire d'´ electrotechnique de Constantine
D´ epartement d' ´ electrotechnique, Universit´ e Constantine 125000, Constantine, Algeria
e-mail: Yassine.MAOUCHE@lec-umc.org

1. INTRODUCTION

Cracked and broken bar in squirrel cage rotor constitutes about 5%-10% of induction motor failures [1]. It can cause torque and speed ripples, decrease average torque, noise and imbalanced stator currents. For these reasons, an amount of papers has been published dealing with broken bar fault detection.

Many researches are based on electrical monitoring that use the induction motor stator currents, known as motor current signature analysis (MCSA) [2] and [3]. These techniques investigate the fault indicative frequencies around fundamental supply frequency or by surveillance of the rotor space harmonic components. But in this case a high sampling frequency value is needed. The main advantage of these techniques is cheap equipment, only one current is needed to detect broken bar fault.

Other researchers have been investigated the influence of broken bar fault on the instantaneous power, activereactive power, instantaneous power factor, torque, external magnetic field analysis, current Park components, inverter input current analysis and supply voltage modulation when the machine is supplied by electrical power converters [4, 5, 6, 7, 8, 9, 10, 11, 12, 13]. These techniques detect the broken bar fault at frequencies close to the dc component in the spectrum $2ksf_s$.

The benefit of these techniques is that the frequency components due to broken bar fault are next to zero frequency and independent of the supply frequency [7].

Several authors apply modern computing approaches, such as genetic algorithm, neural networks, artificial intelligence,wavelet analysis and fuzzy logic [14, 15, 16, 17, 18, 19, 20]. Others propose solutions to on-line condition monitoring with advanced data and signal processing algorithms such as Hilbert method

(HT) [21] and in [22] by using conjugating HT and estimation of signal parameters via rotational invariance technique (ESPRIT) which is superior to MUSIC in both precision and reliability.

All the aforementioned methods become inefficient in the case of low slip, for instance in [6] the broken bar fault is detected only in the frequency range around 300 Hz of the electromagnetic torque spectrum.

On the other hand, the use of $2ksf_s$ close to dc component depends on load level, oscillation load and when using variable speed drives. The aim of this paper is to deal with the first condition with the proposition of a new approach based on calculation and frequency analysis of the partial and total instantaneous power. At the beginning of this study an analytical development of the instantaneous phase and three-phase under healthy condition is presented. The model is based on the winding functions and takes into account the real winding distributions. Then, the harmonic components of instantaneous phase power and instantaneous three-phase power under broken bar fault are analytically analyzed and confirmed by simulation results. Finally, experimental results to validate the proposed method were made under the same conditions for both healthy and faulty induction motor.

The results show a considerable dependence between the load level and the $2ksf_s$ harmonic components in the partial and total instantaneous power spectrums. However the RSH harmonic components induced by broken rotor bar can be used as a fault signature under low slip.

2. HARMONIC COMPONENTS OF INSTANTANEOUS POWER UNDER HEALTHY CONDITION

Suppose a squirrel cage induction machine having symmetrical three-phase system. The rotor cage having n_b bars is viewed as n_b identical spaced loops, and the current distribution can be specified in terms of $n_b + 1$ independent rotor currents.

The stator voltage idn vector matrix from can be written as:

$$[v_s] = [R_s].[I] + \frac{d}{dt}[\psi_s] + [v_n] \tag{1}$$

$$\begin{bmatrix} [v_r] \\ V_e \end{bmatrix} = [0] = \begin{bmatrix} [R_r] & & \frac{R_e}{n_b} \\ & & \vdots \\ \frac{R_e}{n_b} & \cdots & R_e \end{bmatrix} \begin{bmatrix} [i_r] \\ i_e \end{bmatrix} + \frac{d}{dt}[\psi_r] \tag{2}$$

$$[\psi_s] = [L_s][i_s] + [M_{sr}][i_r] \tag{3}$$

$$\begin{bmatrix} [\psi_r] \\ \psi_e \end{bmatrix} = \begin{bmatrix} [M_{sr}].[i_s] \\ 0 \end{bmatrix} + \begin{bmatrix} [L_r] & & \frac{L_e}{n_b} \\ & & \vdots \\ \frac{L_e}{n_b} & \cdots & L_e \end{bmatrix} . \begin{bmatrix} [i_r] \\ i_e \end{bmatrix} \tag{4}$$

Where:

$$[v_s] = \begin{bmatrix} v_{sa} & v_{sb} & v_{sc} \end{bmatrix}^t$$
$$[i_s] = \begin{bmatrix} i_{sa} & i_{sb} & i_{sc} \end{bmatrix}^t$$
$$[\psi_s] = \begin{bmatrix} \psi_{sa} & \psi_{sb} & \psi_{sc} \end{bmatrix}^t$$

are the stator voltage, current and flux vectors respectively.

$[v_r] = \begin{bmatrix} v_{r1} & \cdots & v_{rn_b} \end{bmatrix}^t$, $[i_r] = \begin{bmatrix} i_{r1} & \cdots & i_{rn_b} \end{bmatrix}^t$ and $[\psi_r] = \begin{bmatrix} \psi_{r1} & \cdots & \psi_{rn_b} \end{bmatrix}^t$ are the rotor voltages, current and flux linkage vectors, respectively with dimensions 1 x n_b. $[R_s]$ And $[R_r]$ are the stator and rotor resistance matrices respectively are given by:

$$[R_s] = R_s \cdot [1]_{3x3} \tag{5}$$

$$[R_r] = \begin{bmatrix} 2(R_b+R_e) & -R_b & 0 & 0 & \cdots & -R_b \\ -R_b & 2(R_b+R_e) & -R_b & 0 & \cdots & 0 \\ 0 & -R_b & 2(R_b+R_e) & -R_b & \cdots & 0 \\ 0 & 0 & -R_b & 2(R_b+R_e) & \cdots & 0 \\ \vdots & \vdots & \vdots & \ddots & \ddots & \vdots \\ -R_b & 0 & 0 & \cdots & -R_b & 2(R_b+R_e) \end{bmatrix} \quad (6)$$

$[L_s]$ and $[L_r]$ are the stator and rotor inductance matrices and are described by the same manner as in [9]. $v_n = [v_{o1n1}\ v_{o1n1}\ v_{o1n1}]^t$ is the line neutral voltage taking place between the supply set and the stator set neutral and is given by:

$$v_{o1n1} = \frac{1}{3}(v_{sa} + v_{sb} + v_{sc})$$

As there is no method to infer it, we have to set the stator equations of the model in line-to-line voltage form

$$\begin{bmatrix} v_{sab} \\ v_{sbc} \end{bmatrix} = \begin{bmatrix} R_s & -R_s \\ R_s & 2R_s \end{bmatrix} \cdot \begin{bmatrix} i_{sa} \\ i_{sb} \end{bmatrix} + \frac{d}{dt}\begin{bmatrix} \psi_{sa} \\ \psi_{sb} \end{bmatrix} \quad (7)$$

The zero sequence components corresponding to each stator sets are defined by:

$$\{v_{sa} + v_{sb} + v_{sc} = 3v_{so1} \quad (8)$$

Where:

$$\begin{cases} v_{so1} = \sum_{h=1}^{\infty} V_{soh} \cos(hw_s t + \phi_{vh}) \end{cases}$$

The mutual inductance is calculated using winding function approach includes all the space and rotor harmonics in the machine and its development into Fourier series is given by (9)

$$[M_{sr}] = \sum_{h=1}^{\infty} M_{sr}^{h} \times \begin{bmatrix} \cos(h(\theta+\phi_h)) & \cdots & \cos(h(\theta+\phi_h+ka)) & \cdots \\ \cos(h(\theta+\phi_h-\frac{2\pi}{3})) & \cdots & \cos(h(\theta+\phi_h+ka-\frac{2\pi}{3})) & \cdots \\ \cos(h(\theta+\phi_h+\frac{2\pi}{3})) & \cdots & \cos(h(\theta+\phi_h+ka+\frac{2\pi}{3})) & \cdots \end{bmatrix} \quad (9)$$

where: a = p($2\pi/n_b$) is the electrical angle of a rotor loop.
ϕ_h is the initial phase angle. $k = 1 \ldots n_b$ is a counter of a rotor loop.
When a three-phase induction motor is fed by a symmetrical voltage system a forward rotating field is induced in its air gap. The rotor currents which flow in the rotor loops as a result of the forward field can be expressed as:

$$[i_{rpk}] = \begin{bmatrix} \vdots \\ i_{rpk}\cos(sw_s t - ka - \gamma_p) \\ \vdots \end{bmatrix} \quad (10)$$

Where s is the slip, γ_p is the initial phase angle, and I_{rpk} is the maximum value of the k^{th} rotor loop current.

The instantaneous phase power was used in [8], which is the product of instantaneous line to line voltage and instantaneous line current:

$$p_{int}^{1} = v_{sab} i_{sa} \quad (11)$$

Using (7), (9), (10), (11) and substituting θ by (1- s)$w_s t + \theta_0$ we deduce that:

$$p_{int}^{1} = C_1 + P_0 cos(2w_s - \alpha_0 - pi/6) + \sum_{h}^{\infty}\sum_{k=0}^{n_b} M_{sr}^{h} I_{rpk}\{\tfrac{h}{4}\tfrac{d\theta}{dt} + \tfrac{sw_s}{4}\}\left(\sin(\theta_{(h-(h-1)s\pm1)})\right) + \sum_{h}^{\infty}\sum_{k=0}^{n_b} M_{sr}^{h} I_{rpk}\{\tfrac{h}{4}\tfrac{d\theta}{dt} - \tfrac{sw_s}{4}\}\left(\sin(\theta_{(h-(h+1)s\pm1)})\right) \quad (12)$$

where:

$$\theta_{(h-(h-1)s\pm1)} = (h-(h-1)s\pm1)w_s t + h(\phi_h + \theta_0) + (h-1)ka$$
$$\theta_{(h-(h+1)s\pm1)} = (h-(h+1)s\pm1)w_s t + h(\phi_h + \theta_0)) + (h+1)ka$$

This equation shows that the instantaneous phase power has a component at a double frequency supply, a dc component and a series of high-order components which are induced by the space distribution of rotor bars, and are given by the following:

$$\left\{ h = (\lambda\tfrac{n_b}{p} \pm 1)_{\lambda=1,2...} \cap h = (6\gamma \pm 1)_{\gamma=1,2,3....} \right\} \quad (13)$$

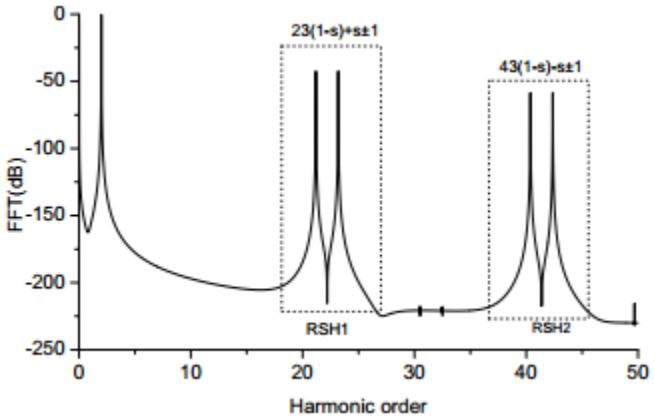

Figure 1. Simulated normalized FFT spectrum of instantaneous phase power of three-phase induction motor under healthy condition

The frequencies of RSHs in the instantaneous phase power are defined by:

$$f_{int}^{1}(h) = (h-(h\pm1)s\pm1)f_s \quad (14)$$

This expression can be rewritten as :

$$f_{int}^{1}(h) = (h(1-s)-s\pm1)f_s \text{ when } h = (\lambda\tfrac{n_b}{p} - 1)$$
$$f_{int}^{1}(h) = (h(1-s)+s\pm1)f_s \text{ when } h = (\lambda\tfrac{n_b}{p} + 1)$$

with orders:

$$h_{pint}^{1} = h \pm 1 \quad (15)$$

Figure 1 shows the spectral content of the simulated instantaneous phase power of the three-phase induction motor under healthy condition. Calculations were made using MATLAB simulation software for three-phase 1.1-kW motor with 24 stator slots and 22 rotor bars, 2 pair poles, and s = 0:03 . When λ = 2, as predicted by equation (13), only one RSH can be seen on the instantaneous phase power spectrum at

$h^1_{pint} = 23 \pm 1$ related to the frequencies $f^1_{int}(23) = (23 - 22s \pm 1)f_s$. The second RSH related to the harmonic order 21 does not show up, which is confirmed by equation (13).

Many papers treated the analysis of total instantaneous power in case of three-phase induction motor defined as :

$$p^3_{int} = v_{sac} i_{sa} + v_{sbc} i_{ba} \tag{16}$$

In same manner as previous, this leads to the following equation:

$$p^3_{int} = C_3 + \sum_{h}^{\infty} \sum_{k=0}^{n_b} M^{3h}_{sr} I_{rpk} \{ \tfrac{3h}{4} \tfrac{d\theta}{dt} + \tfrac{sw_s}{4} \} \left(sin(\theta_{(3h-(3h-1)s\pm3)}) \right) + \sum_{h}^{\infty} \sum_{k=0}^{n_b} M^{3h}_{sr} I_{rpk} \{ \tfrac{3h}{4} \tfrac{d\theta}{dt} - \tfrac{sw_s}{4} \} \left(\sin(\theta_{(3h-(3h+1)s\pm3)}) \right) \tag{17}$$

where

$$\theta_{(3h-(3h-1)s\pm3)} = (3h - (3h-1)s \pm 3)w_s t + 3h(\phi_h + \theta_0) + (3h-1)ka$$
$$\theta_{(3h-(3h+1)s\pm3)} = (3h - (3h+1)s \pm 3)w_s t + 3h(\phi_h + \theta_0) + (3h+1)ka$$

One can notice that the P^3_{int} contains a dc component and a series high-order components which can be defined by the following set:

$$\left\{ h = \frac{1}{3}(\lambda \frac{n_b}{p} \pm 1)_{\lambda=1,2.....} \cap h = (2k+1)_{k=1,2.....} \right\} \tag{18}$$

The frequencies of the instantaneous three-phase power are defined by:

$$f^3_{int}(3h) = (3h - (3h \pm 1)s \pm 3)f_s \tag{19}$$

This equation can be rewritten as

$$f^3_{int}(3h) = (3h(1-s) - s + 3)f_s \text{ when } h = \tfrac{1}{3}(\lambda \tfrac{n_b}{p} - 1)$$

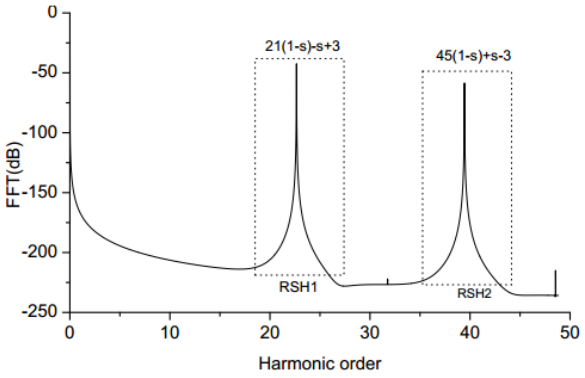

Figure 2. Simulated normalized FFT spectrum of instantaneous three-phase power of three-phase induction motor under healthy condition

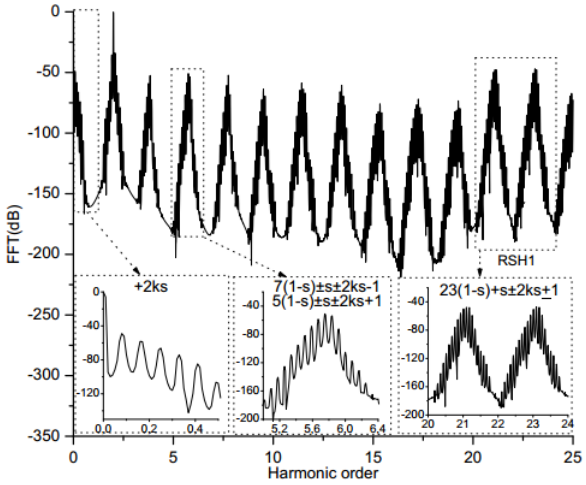

Figure 3. Simulated normalized FFT spectrum of instantaneous three-phase power of three-phase induction motor in faulty condition

$$f_{int}^{3}(3h) = (3h(1-s)+s-3)f_s \text{ when } h = \tfrac{1}{3}(\lambda\tfrac{n_b}{p}+1)$$

with orders

$$h_{pint}^{3} = 3h \pm 3 \tag{20}$$

Figure 2 shows the spectral content of the simulated instantaneous three-phase power of healthy condition. As predicted by (18) the first RSH induced by rotor slot field harmonics corresponds to $h_{pint}^{3} = 21 + 3$ at frequency $f_{int}^{3} = (21 - 22s + 3)f_s$.

3. HARMONIC COMPONENTS OF INSTANTANEOUS POWER UNDER BROKEN BAR CONDITION

A fault on the rotor, such as broken rotor bars causes asymmetrical working. This asymmetry is simulated as a variation in the rotor bar resistance. The maximum values of the rotor loop currents are not equal and the current does not flow through the broken bar.

The rotor broken bar induces additional components in the instantaneous phase power spectrum, and in this case condition (13) becomes:

$$\left\{ h_{pint}^{1} = (6k \pm 1)_{k=1,2,3....} \right\} \tag{21}$$

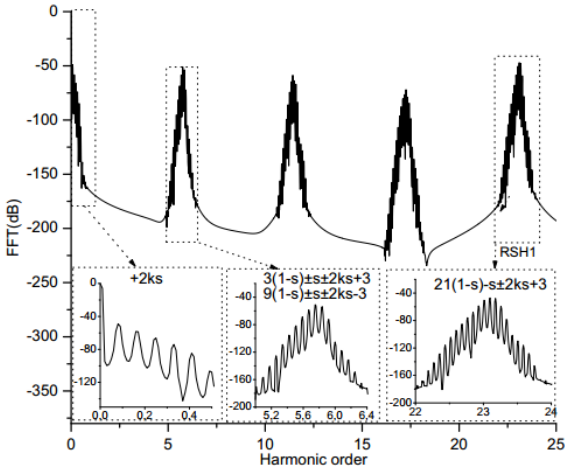

Figure 4. Simulated normalized FFT spectrum of instantaneous three-phase power of three-phase induction motor in faulty condition

And the speed ripples caused by the rotor asymmetry induces other frequencies specified by:

$$f_{int}^{1}(h) = (h(1-s) \pm s \pm 1 \pm 2ks) f_s \tag{22}$$

In the same manner appear new RSH components in instantaneous three-phase power spectrum, their orders are defined by:

$$\left\{ h = (2k+1)_{k=0,1,2,3....} \right\} \tag{23}$$

And the effect of negative sequence induces in rotor currents:

$$f_{int}^{3}(3h) = (3h(1-s) \pm s \pm 3 \pm 2ks) f_s \tag{24}$$

Figures 3 and 4 show the instantaneous phase and three-phase power spectrums under broken bar fault. Conditions (21) and (23) give the order of the supplementary frequency harmonics :

In case of instantaneous phase power spectrum:

$$\left\{ ((1-s) \pm s \pm 1) f_s, (5(1-s) \pm s \pm 1) f_s, (7(1-s) \pm s \pm 1) f_s, (11(1-s) \pm s \pm 1) f_s, , \cdots \right\}$$

In case of instantaneous three-phase power spectrum:

$$\left\{ (3(1-s) \pm s \pm 3) f_s, (9(1-s) \pm s \pm 3) f_s, (15(1-s) \pm s \pm 3) f_s, \cdots \right\}$$

One can notice that there are additional components at the vicinity of harmonics previously mentioned and their frequencies are described by expressions (22) and (24).

4. EXPERIMENTAL VALIDATION

In order to validate the proposed broken bar fault detection model, experimental tests were carried out. The experimental test set-up is shown in Figure 10. Two identical three-phase induction motors have been used, one of them with broken bar fault, and they are rated at 1.1-kW with 24 stator slots, 22 rotor bars, and 2 pair poles, and They were supplied directly from the power line and equipped with voltage and current probes. The load is a magnetic powder brake. The line to line voltages and line currents were recorded by LeCroy scope (WR6050) for a different loads, and sampling frequency for data acquisition is 50 kHz and a

length of 10 s. The instantaneous power is executed by MATLAB software, and then its spectrums were computed by the fast Fourier transform (FFT) of MATLAB software.

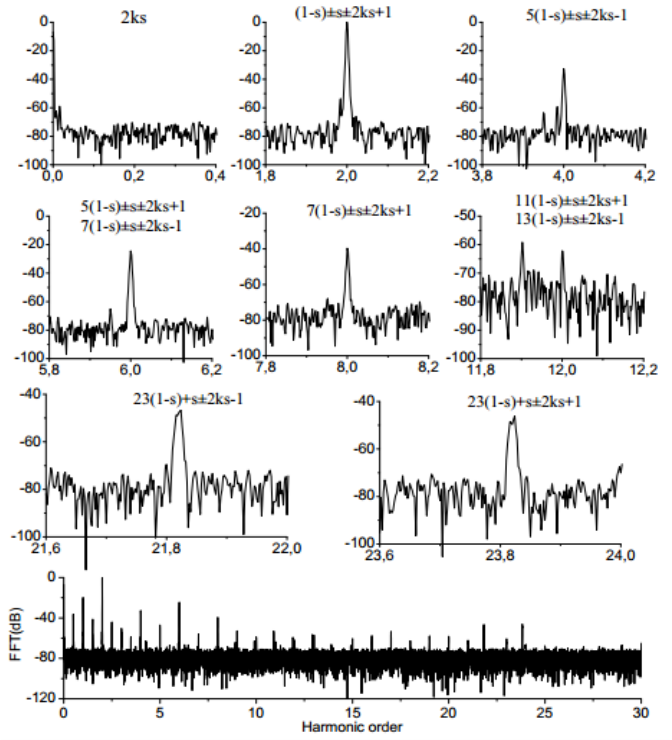

Figure 5. Experimental FFT spectrum of the instantaneous phase power under healthy condition with slip: s = 0.8%

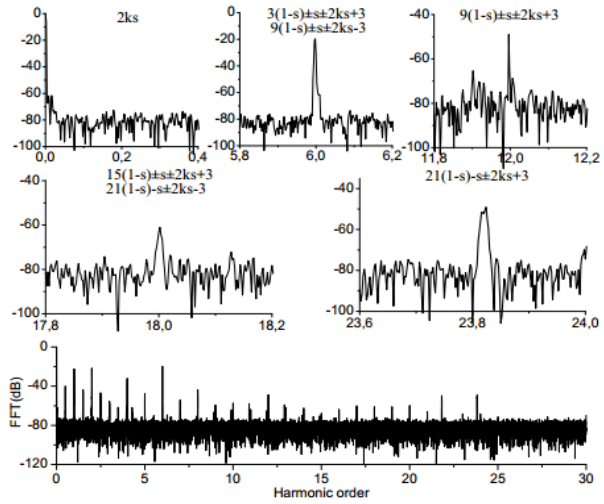

Figure 6. Experimental FFT spectrum of the instantaneous three-phase power under healthy condition with slip: s = 0.8%

In this study, the following cases were investigated:
-At low slip for both conditions (healthy and faulty).
-Under low and high slips for faulty condition.

Figure 5 shows the instantaneous phase power spectrum under healthy condition at 0.8% slip. In this case the time harmonic frequencies become 2 γfs and the first RSH harmonic frequencies are (23 - 24s ± 1)fs.

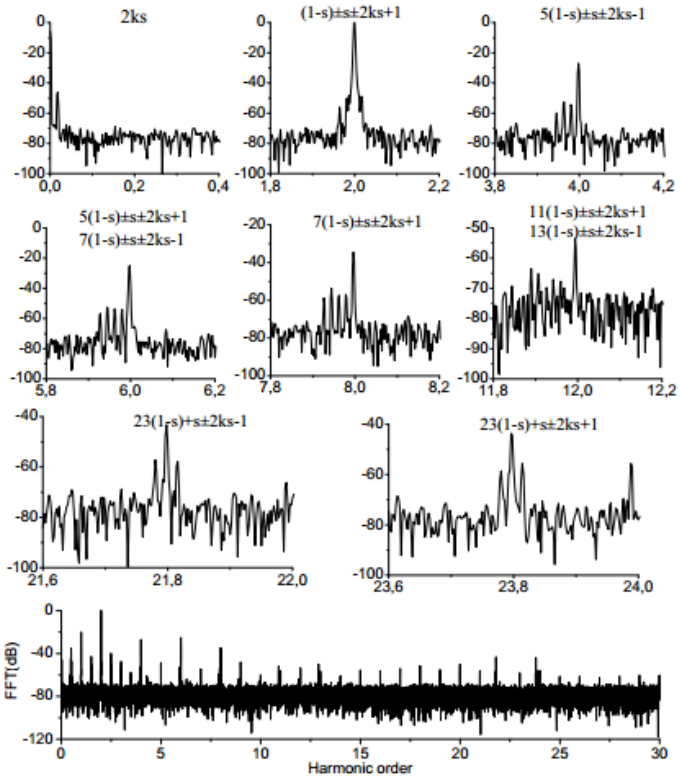

Figure 7. Experimental FFT spectrum of the instantaneous phase power under faulty condition with slip: s = 0.8%

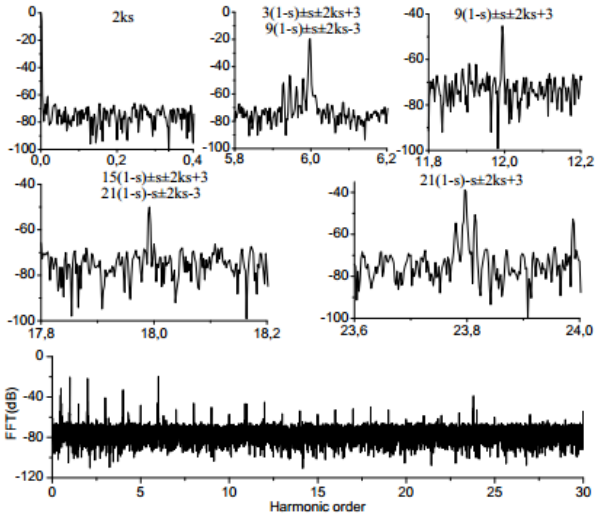

Figure 8. Experimental FFT spectrum of the instantaneous three-phase power under faulty condition with slip: s = 0.8%

Figure 6 shows the spectrum of the instantaneous three-phase power under healthy condition. Additional to the dc component appear the time harmonics at frequencies 3γfs and the first RSH

corresponding to λ = 2 at frequency (21 - 22s + 3)f_s. Both instantaneous three-phase and phase power spectrums confirm the simulation and analytic results.

Figure 8 shows the spectrum of instantaneous three-phase power under broken bar fault. One can notice that: a total absence of the 2ksf_s harmonics close to the dc component, on the contrary the frequencies (3(1 - s) ± s ± 2ks + 3)f_s and (9(1 - s) ± s ± 2ks - 3)f_s close to the sixth harmonic order appear in clear manner and they have an important magnitudes. This makes them a potential broken bar fault signature in instantaneous three-phase spectrum at low slip.

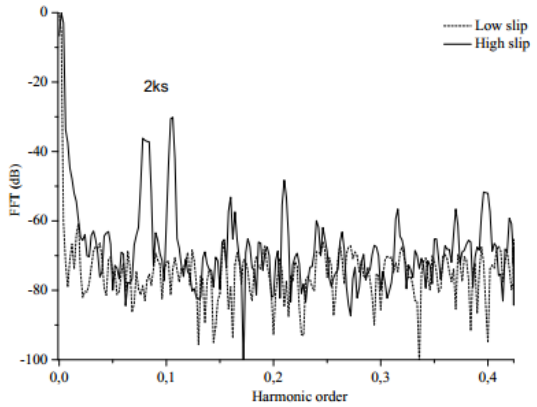

Figure 9. Experimental FFT spectrum of the instantaneous three-phase power under broken bar fault with low and high slip

Figure 10. View of the experimental test set-up system

Next to the RSH frequencies (21- 20s ± 3)f_s appear a side-band frequencies (21 - 20s + 3 ± 2s)f_s induced by speed ripple.

Figure 7 presents the spectrum of instantaneous phase power under broken bar fault. One can notice the appearance of a 2sf_s harmonic component located next to the dc component. However the harmonic (1- 2s + 1)f_s does not appear as same as the 2sf_s component in the three-phase instantaneous power spectrum. On the other hand, one can observe the presence of the analytically predicted harmonics at frequencies (5(1 - s) ± s ± 1)f_s and (7(1 - s) ± s ± 1)f_s, and these are the most prominent components induced by broken bar fault in instantaneous phase power spectrum at low slip.

It is obvious that RSH harmonics with higher frequencies induced by broken bar fault in both instantaneous phase and three-phase power spectrums are more reliable under low slip. However in instantaneous phase spectrum there is more than one significant signature under low slip, and this enhances the conclusion that the use of more than one signature strengthens the fault detection method.

Figure 9 shows the instantaneous three-phase power spectrum under broken bar fault of both high and low slips. One can see the existence of $2ksf_s$ harmonics at high slip. However, at low slip the $2ksf_s$ harmonics are not identifiable and are masked by floor-noise level. It is clear that the traditional diagnostic method depends strongly on the slip level, and it would be necessary to use the RSH harmonics with higher frequencies at low slip.

5. CONCLUSION

In this paper, analytical study proved by simulation results of the influence of broken bar fault in instantaneous phase and three-phase power spectrums was presented. The considered model in this paper is able to show the impact of broken bar fault in instantaneous power spectrum, but it is not able to clarify the influence of load on the appearance of the fault signatures, and this is because the used model does not take into account the exact geometrical representation of the induction machine (stator slots opening, skewing effect etc....). The experimental results clearly show that under broken bar fault and with low slip the RSH harmonics at low frequencies range in instantaneous phase and three-phase power can not be reliably detected. However, the proposed method based on RSH harmonics works reliably at high frequencies range when the slip is small. At small slip range the more reliably induced RSH harmonics due to broken bar fault are given by:

In instantaneous phase power spectrum mainly into:

The first before the sixth and eighth time harmonics.

The second next to the first RSH harmonic appear a side-band frequencies.

In instantaneous three-phase power spectrum mainly into:

The first before the sixth time harmonics.

The second next to the first RSH harmonic appear a side-band frequencies.

REFERENCES

[1] S Nandi, et al. "Condition monitoring and fault diagnosis of electrical motors-a review". *IEEE Transactions Energy Conv*. 2005; 20(4): 719729.

[2] A Khezzar, et al. "On the Use of Slot Harmonics as a Potential Indicator of Rotor Bar Breakage in the Induction Machine". *IEEE Transactions Ind. Electron*. 2009; 56(11): 4592 – 4605.

[3] SH Kia, et al. "A high-resolution frequency estimation method for three-phase induction machine fault detection". *IEEE Transactions. Ind. Electron.* 2007; 54(4): 23052314.

[4] M Drif and A Cardoso. "Discriminating the simultaneous occurrence of three-phase induction motor rotor faults and mechanical load oscillations by the instantaneous active and reactive power media signature analyses". in *IEEE Transactions Ind. Electron*. 2012; 59(3): 1630-1639.

[5] M Nemec, et al. "Detection of broken bars in induction motor through the analysis of supply voltage modulation". in *IEEE Transactions Ind. Electron.* 2010; 57(8): 2879-2888.

[6] KN Gyftakis, et al. "A Novel Approach for Broken Bar Fault Diagnosis in Induction Motors Through Torque Monitoring". in *IEEE Transactions in Energy Conversion.* 2013; 28(2): 267 – 277.

[7] M Eltabach, et al. "*Detection of broken rotor bar of induction motors by spectral analysis of the electromagnetic torque using luenberger observer*". in Proc. IEEE 27th Annu. Conf. Ind.Eletron. Soc., Denver, CO, USA. pp.658-663 Nov. 29 Dec. 02, 2001.

[8] C Kral, et al. "*A comparison of rotor fault detection techniques with respect to the assessment of fault severity*". in Proc. SDEMPED, Atlanta, GA. 2003: 265-270.

[9] A Khezzar, et al. "*Analytical investigation of rotor slot harmonics in a three phase induction motor with broken rotor bars*". in Proc. EPE, Dresden, Germany. 2005.

[10] J Faiz and M Ojaghi. "Instantaneous-power harmonics as indexes for mixed eccentricity fault in mains-fed and open/closed-loop drive-connected squirrel-cage induction motors". in *IEEE Trans. Ind. Electron.* 2009; 56(11): 47184726.

[11] SMA Cruz. "An Active Reactive Power Method for the Diagnosis of Rotor Faults in Three-Phase Induction Motors Operating Under Time- Varying Load Conditions". in *IEEE Transactions on Energy Conversion.* 2012; 27: 71-84.

[12] A Ceban, et al. "Study of Rotor Faults in Induction Motors Using External Magnetic Field Analysis". in *IEEE Transactions Industrial Electronics*. 2012; 59(5): 20822-22093.

[13] AM da Silva, et al. "Induction machine broken bar and stator short-circuit fault diagnostics based on threephase stator current envelopes". in *IEEE Trans. Ind. Electron.* 2008; 55(3): 13101318.

[14] CM Pezzani, et al. "*A new approach to the Parks vector for broken bars and load oscillation diagnosis on IM*". in Proc. IEEE 9th Int. Conf. Ind. Technol. Vi na del Mar, Chile. 2010: 12211226.

[15] VN Ghate and SV Dudul. "Cascade Neural-Network-Based Fault Classifier for Three-Phase Induction Motor", in *IEEE Transactions on Industrial Electronics*. 2011; 58: 1555-1563.

[16] AK Mahamad and T Hiyama Dudul. "*Improving Elman network using genetic algorithm for bearing failure diagnosis of induction motor*". in Proc. IEEE SDEMPED. 2009: 1-6.

[17] J Pons-Llinares, et al. "*Induction motor fault diagnosis based on analytic wavelet transform via frequency Bsplines*". in Proc. IEEE SDEMPED. 2009; 1-7.

[18] MBK Bouzid, et al. “An effective neural approach for the automatic location of stator inter-turn faults in induction motor”. in *IEEE Trans. Ind. Electron*. 2008; 55(12): 4277-4289.
[19] Z Gao, et al. “Novel parameter identification by using a high-gain observer with application to a gas turbine engine”. in *IEEE Transactions on Industrial Informatics*. 2008; 4: 271-279.
[20] CH Lu. “Wavelet fuzzy neural networks for identification and predictive control of dynamic systems”. in *IEEE Trans. Ind. Electron*. 2011; 58(7): 3046-3058.
[21] P Puche-Panadero, et al. “Improved resolution of the MCSA method via Hilbert transform, enabling the diagnosis of rotor asymmetries at very low slip”. in *IEEE Trans. Energy Convers*. 2009; 24(1): 5259.
[22] B Xu, et al. “Improvement of the Hilbert Method via ESPRIT for Detecting Rotor Fault in Induction Motors at Low Slip”. in *IEEE Trans. Energy Convers*. 2013; 28(1): 225-233.